Asian Journal of Chemistry; Vol. 37, No. 9 (2025), 2281-2290
ASIAN JOURNAL OF CHEMISTRY
https://doi.org/10.14233/ajchem.2025.34002

Effectiveness of African Wattle Tree (*Peltophorum africanum*) Biochar in Removing Carmoisine Dye from Wastewater

CHRISTINE BURUKAI[1], BOTHWELL NYONI[1,2,*], DORCAS NYAMA[1], CLEVER MPOFU[1], BONGIBETHU HLABANO-MOYO[3], BONGANI YALALA[1], JABULANI I. MNYANGO[2] and SHANGANYANE P. HLANGOTHI[2]

[1]Department of Applied Chemistry, National University of Science and Technology, Bulawayo, Zimbabwe
[2]Centre for Rubber Science and Technology, Department of Chemistry, Nelson Mandela University, Gqeberha, South Africa
[3]Department of Civil Construction and Environmental Engineering, Iowa State University, Iowa, USA

*Corresponding author: E-mail: s215391977@mandela.ac.za; bothwell.nyoni@nust.ac.zw

Received: 6 May 2025 *Accepted*: 20 August 2025 *Published online*: 30 August 2025 AJC-22110

In this work, the use of biochar synthesized from the African wattle tree (*Peltophorum africanum*) bark as an adsorbent for the removal of carmoisine, a common red azo dye from a simulated effluent, is investigated. The study focuses on the effect of adsorbent synthesis conditions, particularly the carbonization temperature, then, the adsorption process conditions and finally, analyzing the relevant isotherms, kinetics and mechanisms. It was revealed that the point of zero charge for the activated biochar prepared at 500, 600 and 700 ºC were 6.6, 6.5, and 6.3 respectively, indicating that the surface charge of the adsorbent became more positive as temperature was increased. Consequently, all adsorbent samples displayed a decrease in removal efficiency when the pH of the solution increased. Adsorption experiments revealed that the process best fits the Langmuir isotherm model with monolayer adsorption capacities of 49.8, 56.1 and 63.8 mg g^{-1} for activated biochars prepared at 500, 600, and 700 ºC, respectively. Kinetics studies further reveal that the adsorption process generally follows pseudo-second-order kinetics with k_2 values in the range of 0.01–0.1 min^{-1}. The most probable adsorption mechanisms involve hydrogen bonding and electrostatic interactions due to the presence of carbon-oxygen and carbon-nitrogen functional groups.

Keywords: Azo dye, Biochar, Carmoisine, Isotherms, Water purification, Wattle tree bark.

INTRODUCTION

Effluent discharge from industrial activities is one of the major contributors to pollution in rivers and water bodies that are located nearby urban industrial areas. The residual dyes are the organic chemicals and have a complex aromatic molecular structure, which is based on substituted aromatic and heterocyclic groups and are generally resistant to light, temperature, biodegradation, ozonation and oxidation [1]. This characteristic feature makes dyes non-degradable and therefore causes bioaccumulation in living organisms, leading to severe diseases and disorders [2,3]. In addition, dyes may have acute or chronic effects on aquatic organisms. Similarly, toxic dyes can enter the food chain through water bodies, eventually affecting the health of land lifeforms. Several studies have demonstrated the allergenic, clastogenic, mutagenic and carcinogenic effects of different dyes such as tartrazine, Allura red, Amaranth, carmoisine and brilliant blue [4-6]. Many classifications are used to differentiate azo dyes; however, they are commonly classified as disperse, metal-complexes, reactive, and substantive dyes [7]. Carmoisine is an azo dye that is commonly used particularly in jewellery, cosmetics, foods, and ink. Carmoisine dye also has several uses in artwork, including paintings, posters and stained-glass windows. Its use is highly regulated in several developed countries since of its carcinogenic effects; however, this is not the case in underdeveloped countries [8,9].

There are several methods for the removal of dyes from industrial effluents. The methods can be categorized into physical, chemical and biological treatment processes. These include adsorption, flotation, electro-flotation, flocculation with Fe(II) and $Ca(OH)_2$, membrane-filtration, electrokinetic coagulation, precipitation, ozonation and the Katox treatment method that involves the use of activated carbon and air

mixtures [10]. Biological processes include the use of microorganisms such as bacteria, yeast, algae, and fungus that can collect and break down different dyes [11].

Mathur *et al.* [12] studied the use of *Lentinus squarrosulus* AF5 strain in the remediation of textile azo dyes *via* catabolism, in particular amido black 10B, reactive black 5 and reactive blue 160. The isolated *Lentinus squarrosulus* AF5 was assessed for decolourization and showed approximately 93, 88 and 70 % decolorization of reactive blue 160, reactive black 5, and amido black 10B, respectively. Labiod *et al.* [13] evaluated the removal of carmoisine by adsorption process using natural diatomite, which was mainly composed of silica. The study managed to show that at room temperature and optimal experimental conditions, the highest adsorption capacity of 12 mg/g was obtainable at a colorant concentration of 50 mg/L, pH of 2, contact time of 30 min and diatomite concentration of 1 g/L. Modelling studies showed that experimental results fitted the Freundlich isotherm in multilayer adsorption. The adsorption data fitted pseudo-second-order kinetics and the thermodynamic parameters indicated that the nature of the adsorption process is endothermic and spontaneous.

Various approaches for the remediation of dyes from industrial effluents are currently under investigation. In this study, we evaluate the effectiveness of low-cost activated carbon synthesized from the bark of the African wattle tree (*Peltophorum africanum*) as an adsorbent for the removal of carmoisine dye. The African wattle tree is widely available, easy to cultivate, and its carbon-rich bark provides a promising material with high adsorptive capacity. The production of activated carbon from inexpensive, renewable resources, such as the bark of African wattle tree, provides a viable and environmentally responsible substitute for traditional adsorbents. Furthermore, other studies have demonstrated the potent adsorption capabilities of activated carbons and biochars made from a variety of plant materials, indicating that the African wattle tree may offer a useful medium for eliminating artificial dyes like carmoisine from tainted water, thereby supporting eco-conscious water treatment methods. Adsorbent samples were synthesized at different temperature conditions followed by physico-chemical characterization. The main parameters for controlling the adsorption treatment process were optimized in batch adsorption experiments. Finally, modelling of adsorption isotherm and kinetics was performed.

EXPERIMENTAL

The required chemicals and solvents were of AR grade and purchased from different commercial sources. Carmoisine dye was purchased from a local dye supplier, Bulawayo, Zimbabwe. Fourier transform infrared (FTIR) analysis of the dye and adsorbents was performed using a Bruker (USA), Tensor 27 spectrometer. Samples were scanned in the wavelength range of 400-500 cm^{-1}. The pH of the dye solution at different temperatures was measured by use of pH and temperature probes for the temperature range of 20-60 ºC. The pH of distilled water was used as a reference point. To determine the pH at the point of zero charge (pH_{pzc}) of the adsorbents, from 50 mL of 0.1 M sodium nitrate solutions kept in separate beakers, a mass of 0.1 g of adsorbent sample was added to each beaker. The suspension was stirred for 24 h at a speed of 200 rpm. The final pH was measured to determine the pH_{pzc} by means of plots of ΔpH *versus* the initial pH.

Preparation of dye and adsorbent: The simulated effluent was prepared by dissolving carmoisine dye powder in distilled water to make a stock solution of 150 ppm. Aliquot solutions were prepared by diluting the stock solution as required. Wood from African wattle tree (*Peltophorum africanum*) was collected from the Midlands province of Zimbabwe. The bark from the wood was peeled using a knife and was left to dry in the sunlight for 72 h. The bark was ground using pestle and mortar. The powder was sieved using a No. 10 mesh testing sieve. A 100 g of tree bark powder was washed with distilled water at 80 ºC, followed by ethanol (96 %, Sigma-Aldrich, Germany) at 60 ºC. The precursor material was filtered and dried in an oven at 105 °C for 24 h. The activating agent used was 40 % H_3PO_4 with three parts added to one part of the precursor material. The resultant mixture was stirred for 2 h under constant agitation speed of 200 rpm. Drying was carried out by use of an oven with a set temperature of 105 ºC for 12 h. Samples of African wattle tree activated biochar (AWAB) adsorbent were obtained by carbonizing in a muffle furnace for 2 h at various temperatures of 500, 600, and 700 ºC. Distilled water was used to rinse the resultant AWAB until a sample with a neutral pH was obtained. The final AWAB samples were then dried at 105 ºC for 6 h and kept in an airtight bottle for use in characterization and adsorption tests.

Adsorption experiments: The adsorption analyses were conducted in batch mode at ambient temperature. A known amount of adsorbent was added to a solution of known concentration. The mixture was agitated for a certain amount of time in an orbital shaker at a speed of 200 rpm. Process variables like dye concentration, initial pH of solution, amount of adsorbent added and contact time where measured. Aliquots were extracted from the solutions before and after the adsorption process. The adsorbent was filtered out of the solution, dried, and characterized using the FTIR spectroscopy. The solution samples were studied for absorbance measurements using a single-beam type UV/visible spectrophotometer. The prepared effluent solution was scanned in the visible spectrum between 400 and 800 nm to determine the maximum wavelength of 512 nm. The calibration was conducted at this wavelength for all the concentrations. The correlation coefficient of the calibration curve was 0.996.

The percentage (%) dye removal and adsorption capacity q (mg/g) were calculated according to eqns. 1 and 2 as follows:

$$\text{Removal (\%)} = \frac{C_o - C_f}{C_o} \times 100 \quad (1)$$

$$q = \frac{(C_o - C_f)V}{m} \quad (2)$$

where C_o and C_f are the initial and final concentrations (ppm) of carmoisine dye in solution; V is the volume (L) of the solution containing carmoisine dye; and m (g) is the mass of the adsorbent.

Adsorption isotherms and kinetics analysis: The two commonly adsorption isotherm models *i.e.* Langmuir and Freundlich models, and two kinetic models, *i.e.* pseudo-first

and second order models were investigated using eqn. 3-6, respectively [14,15].

$$q_e = \frac{q_m K_L C_e}{1 + a_L C_e} \quad (3)$$

$$q_e = K_F C_e^{a_F} \quad (4)$$

$$q_t = q_e(1 - e^{k_1 t}) \quad (5)$$

$$q_t = \frac{q_e^2 k_2 t}{1 + k_2 q_e t} \quad (6)$$

where q_e are q_m (mg/g) represent the quantity of dye adsorbed at equilibrium and maximum capacity, respectively. K_L (L/mg) and a_L (L/mg) are the Langmuir isotherm model constants, K_F (L/mg) and a_F are the Freundlich isotherm constants, k_1 (min^{-1}) and k_2 (g/mg·min) are the pseudo-first and second order kinetics model constants, respectively. To reduce the discrepancies due to propagation errors, both linear and non-linear forms of the models were evaluated. The models are presented in Table-1.

RESULTS AND DISCUSSION

Knowledge of the functional groups present in the carmoisine dye and adsorbent materials is vital in order to understand and improve the process of adsorption. Fig. 1 shows the FTIR spectra of carmoisine dye (a) and AWAB (b) synthesized at 700 ºC. No any distinct differences in functional groups among AWAB samples synthesized at different temperatures were revealed. The spectrum for carmoisine dye displays strong peaks at 413, 544, 620, 648, 683, 759, 946, 1010, 1046, 1178, 1278, 1370, 1501, 1607, 3075 and 3433 cm^{-1}. Carmoisine dye is composed of disodium 4-hydroxy-3-(4-sulphonato-1-naphthylazo)naphthalene-1-sulphonate and subsidiary coloring matters, along with sodium chloride and/or sodium sulphate as the primary uncoloured components [16]. The peaks at 413, 544 and 1046 cm^{-1} correspond to the symmetric vibrations of the SO_3 bonds from the sulphonic acid salts of the $R–SO_3^-M^+(Na^+)$ group, in-plane deformation vibrations of the aromatic =C–H bonds of the 1,2-disubstituted benzene and vibrations of in-plane deformation of the aromatic ring bonds, respectively. The peaks at 620, 759, 946, 1010, 1278, and 2090 cm^{-1} are attributed to the in-plane deformation vibrations of the aromatic =C–H bonds of the 1,4-disubstituted and 1,2,4-trisubstituted benzenes. The peak at 1370 cm^{-1} corresponds to the vibrations of the bonds of the S=O and C–S groups. The peak at 1501 cm^{-1} corresponds to the stretching vibrations of the N=N bond of the aromatic azo group and the aromatic ring C=C stretching vibrations. The peaks at 683, 3075 and 3433 cm^{-1} correspond to the vibrations of the hydroxyl group (–OH).

The synthesized adsorbent (AWAB) possessed functional groups characteristic of common, inexpensive adsorbents that are synthesized from lignocellulosic precursor materials. The peak at 1720 cm^{-1} corresponds to the bond stretching vibrations of the C=O present in aliphatic ketones and carboxylic acids. The major peak at 1552 cm^{-1} is attributed to the C=C bond stretching vibrations of aromatic rings of sp^2 graphite. The two peaks at 2986 and 1140 cm^{-1} correspond to C–H and C–O vibrations of methyl and alkoxyl groups, respectively [17]. It has been reported that a broad peak in the 1200–1000 cm^{-1}

TABLE-1
SELECTED MODELS FOR ANALYZING ADSORPTION OF CARMOISINE DYE [15]

Model		Plot (y *vs.* x)	Evaluated constants
Langmuir isotherm	Linear	$\frac{1}{q_e}$ *vs.* $\frac{1}{C_e}$	K_L (L/mg); q_m (mg/g)
	Non-linear	q_e *vs.* C_e	K_L (L/mg); q_m (mg/g)
Freundlich isotherm	Linear	log q_e *vs.* log C_e	K_F (mg/g), b_F
	Non-linear	q_e *vs.* C_e	K_F (mg/g), b_F
Pseudo-first-order kinetics	Linear	log ($q_e - q_t$) *vs.* t	k_1 (min^{-1})
	Non-linear	q_t *vs.* t	k_1 (min^{-1})
Pseudo-second-order kinetics	Linear	t/q_t *vs.* t	k_2 (g/mg.min)
	Non-linear	q_t *vs.* t	k_2 (g/mg.min)

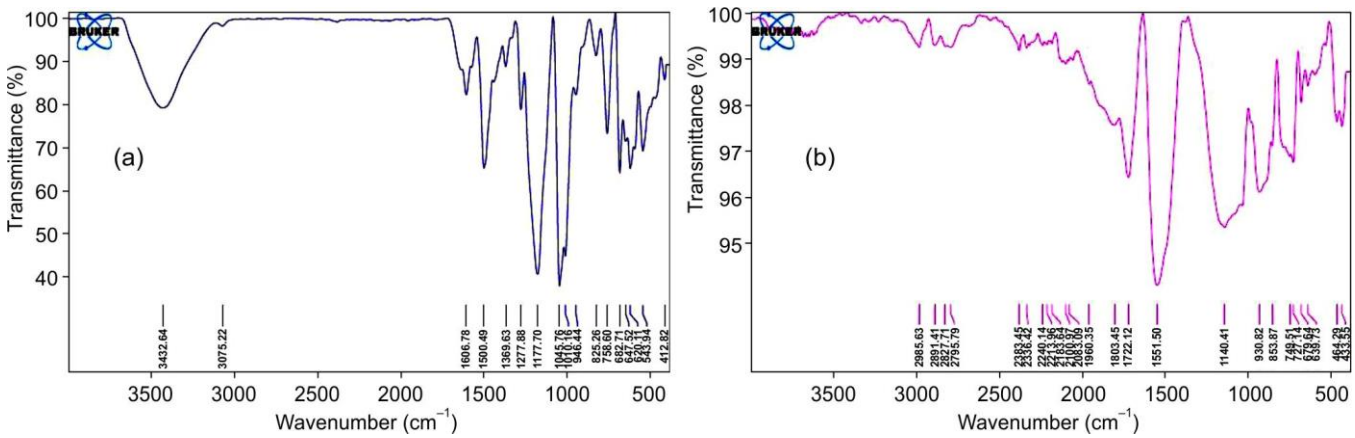

Fig. 1. FTIR spectra for (a) carmoisine powder and (b) AWAB prepared at a carbonization temperature of 700 °C

region can arise due to other functional groups such as inorganic and organic silicon, phosphorus compounds and sulphate groups which are normally present in biochar [18]. The broad peak in the range of 931-854 cm^{-1} corresponds to the C–H and C=C bond bending vibrations present in 1,2,4-trisubstituted benzenes and monosubstituted alkenes, respectively. The peaks at 434 and 464 cm^{-1} correspond to bond stretching of C-X (X = halogen) and halogen atoms in halo compounds and vibrations of in-plane deformation of the =C–H bonds in aromatic rings. Some peaks appear in the range of 2383-2083 cm^{-1}, which correspond to N=C=N and C=O bond stretching vibrations from carbodiimide groups [19]. The weak peaks in the range of 3400-3200 cm^{-1} correspond to N–H stretching vibrations of amine groups.

The interactions between the R–SO_3^-, –N=N, –S=O and –C–S groups in carmoisine dye with the R–O–H, R–C=O, R–N–H, R–N=C=N–R groups that are present on the surface of the AWAB are among the most important driving forces for the adsorption process [19-22]. Several adsorption mechanisms indicate that O–H and C=O groups participate in adsorption *via* hydrogen bonding with other functional groups in solution.

Effect of pH: The dependence of pH of the dye solution on temperature is shown in Fig. 2. At 20 ºC, the dye solution has a weak alkaline character, corresponding to a pH 7.2 and as the temperature increases, the acidity of the solution increases, the pH reaching a value of 6.6 at 60 ºC. This information, along with the point of zero charge of the adsorbent, is vital in setting up an adsorption process. The point of zero charge (pzc) is the pH at which the net electrical charge of the adsorbent's surface is equal to zero. The pzc curves for the different samples of adsorbents are shown in Fig. 3. The pH at the point of zero charge (pH_{pzc}) was determined as the pH value. For the adsorbent carbonized at 500, 600, and 700 ºC, the pH_{pzc} values were found to be pH 6.6, 6.5 and 6.3, respectively. The surface of all the adsorbent samples is positively charged as evidenced by their pH_{pzc} values, which are predominantly below pH 7, which makes the adsorbent suitable for the adsorption of carmoisine dye at temperatures less than 40 ºC, where the solution will be predominantly negatively charged. At these temperatures, carmoisine dye normally dissociates in aqueous solution to form R–SO_3^- anions [23]. The results from pzc determination are comparable with results from other studies where low-cost adsorbents were studied

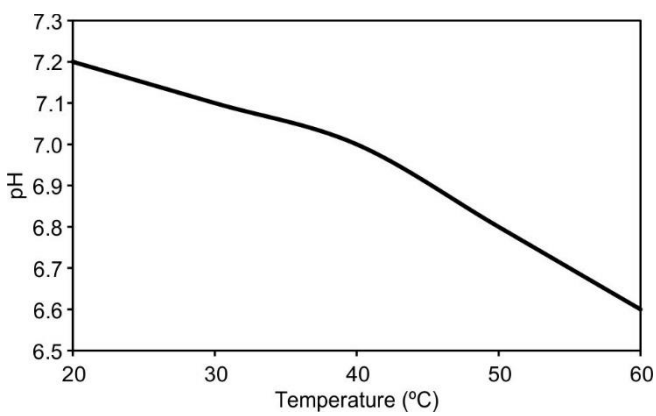

Fig. 2. pH variation of dye solution with temperature

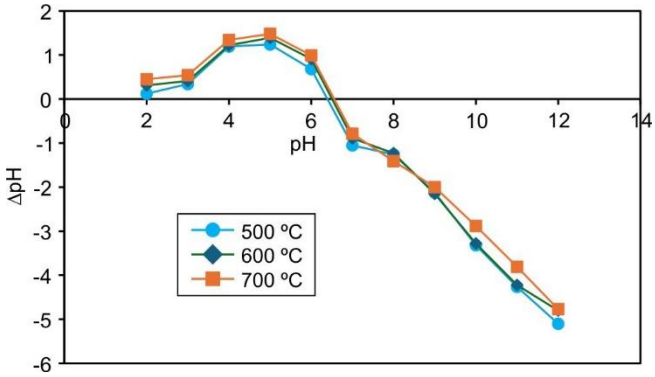

Fig. 3. Point of zero curves for adsorbents prepared at different carbonization temperatures

[21,24]. There is a decrease in pH_{pzc} as the temperature of carbonization is increased, and this may be attributed to the enhanced decomposition of alkaline functional groups and an increase in cross-linking reactions that form acidic char [25].

Adsorption studies

Effect of initial adsorbent dosage: Adsorption studies to determine the effect of adsorbent dosage were carried out using an initial carmoisine concentration of 120 ppm at pH 2 and a contact time of 60 min. Visual observations confirmed the degradation in the dye colour as the dosage was increased (Fig. 4). Furthermore, from Fig. 5, it is shown that the % dye removal increases with an increase in adsorbent dosage as expected. As the amount of adsorbent is increased, active sites for adsorption are increased, thereby enhancing the removal of dye. The adsorbent synthesized by carbonizing at 700 ºC displayed the highest removal efficiency at all dosage levels.

Fig. 4. Colour of solutions resulted after adsorption with a known amount of adsorbent 1. 0 g, 2. 0.02 g, 3. 0.08 g, 4. 0.1 g, and 5. 0.12 g

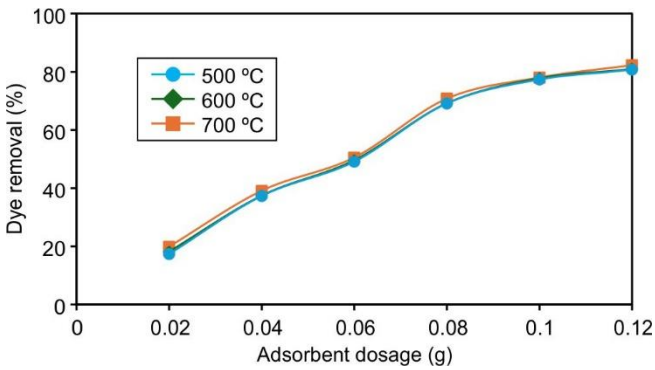

Fig. 5. Effect of initial dosage on adsorption of carmoisine dye using AWAB synthesized from different temperature

Effect of initial dye concentration: The concentration range explored was in the range of 50-150 ppm using a fixed adsorbent dosage of 0.12 g and a solution pH of 2. The effect of initial dye concentration is shown in Fig. 6. It is apparent that as the initial concentration of carmoisine dye increased the % dye removal for all the adsorbent samples. At low concentrations of dye, there are enough adsorption sites for the uptake of the few dye molecules; therefore, the removal efficiency is high. However, as the concentration is increased, the adsorbent sites get saturated resulting in excess dye molecules remaining in the solution. It is evident that the adsorbent synthesized at 700 ºC had better removal efficiency for a concentration range of 50-100 ppm. In other words, there is an observed increase in dye removal efficiency with carbonization temperature.

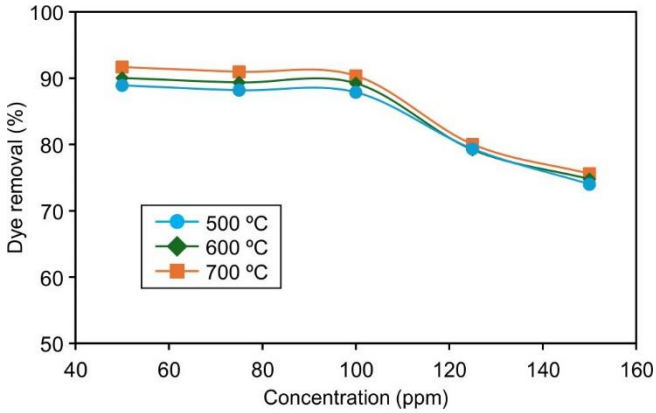

Fig. 6. Effect of initial dye concentration on adsorption of carmoisine dye using AWAB synthesized from different temperature

Effect of initial pH: The effect of the initial pH of carmoisine dye solution was carried out by varying the pH from 2 to 10 *via* the addition of 0.1 M HCl or NaOH. The observation shows that as the initial pH of the carmoisine dye solution increases, the % dye removal decreases for all the adsorbents. This implies that the adsorbents are effective in acidic conditions. This trend is supported by the pH_{pzc} results presented earlier. The pH_{pzc} for the adsorbents was reported to be in the range of 6.3 to 6.6 (Fig. 7). This implies that in cases where the solution has a pH < pH_{pzc}, the adsorbent surfaces are predominantly positively charged, thereby attracting more R–SO_3 groups from the dye in solution *via* either hydrogen bonding, van der Waals forces or electrostatic interactions. However, for solution pH > pH_{pzc}, the surface charge becomes negative with repulsive forces that greatly reduce the dye removal efficiency. Furthermore, at high pH, the presence of more –OH ions result in competition with R–SO_3^- ions, thereby reducing their uptake efficiency. The observations are consistent with literature where low-cost adsorbents synthesized from lignocellulosic biomass were explored [15,26,27]. The adsorbent that underwent carbonization at 70 ºC displayed an improved adsorption efficiency.

Effect of contact time: Understanding the effect of contact time is important in the study of adsorption kinetics and scale-up. The experiments were carried out using an initial dye concentration of 120 ppm, an adsorbent dosage of 0.12 g and a solution pH of 2. The effect of contact time is presented

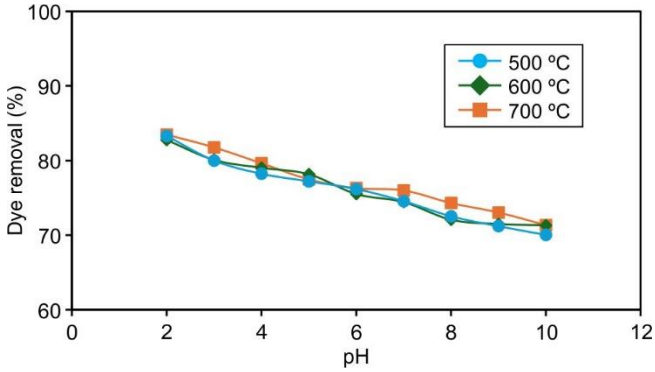

Fig. 7. Effect of pH on adsorption of carmoisine dye using AWAB synthesized from different temperature

in Fig. 8, where the dye removal efficiency is seen to increase as the contact time increases in the range of 10-40 min. There is a rapid increase in removal efficiency in the first 25 min, followed by a slow increase until approximately 50 min for the two adsorbents synthesized by carbonizing at 500 and 600 ºC. A further increase in contact time beyond 50 min results in no further significant increase in efficiency. Therefore, it can be deduced that for the two adsorbents, the time for the adsorbents to reach equilibrium is 50 min; at this point, the adsorbent reaches saturation. However, the adsorbent synthesized at 700 ºC displays improved the adsorption capabilities because the adsorption reaches equilibrium at approximately 35 min with the highest removal.

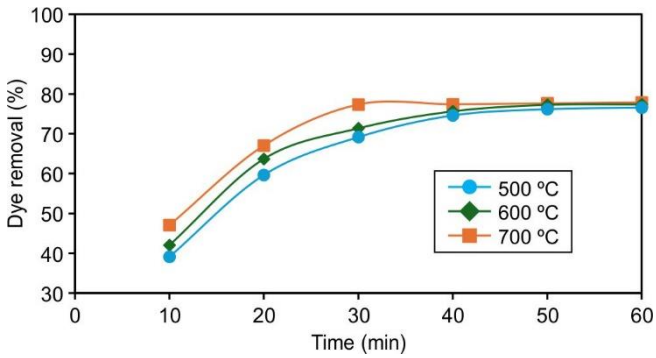

Fig. 8. Effect of contact time on adsorption of carmoisine dye using AWAB synthesized from different temperature

Isotherms studies: Adsorption experiments were carried out at ambient temperature and optimal conditions were determined as pH = 2, adsorbent mass = 0.12 g, and contact time = 50 min, using an adsorbent sample. Adsorption isotherms and their parameters were determined by means of linear and non-linear plots as previously illustrated in Table-1. Linear and non-linear plots for Langmuir and Freundlich isotherms were prepared according to the method of Hossain *et al*. [28]. The plots for activated carbon synthesized at 700 ºC are shown in Figs. 9 and 10 for Langmuir and Freundlich models, respectively.

The evaluated parameters for the two models are shown in Table-2. The adsorption data have a better fit for Langmuir isotherm as evidenced by the high R^2 values. Furthermore, the R^2 values for the Langmuir linear and non-linear models are in better agreement. If the adsorption of carmoisine dye follows the Langmuir isotherm, the model parameters evalu-

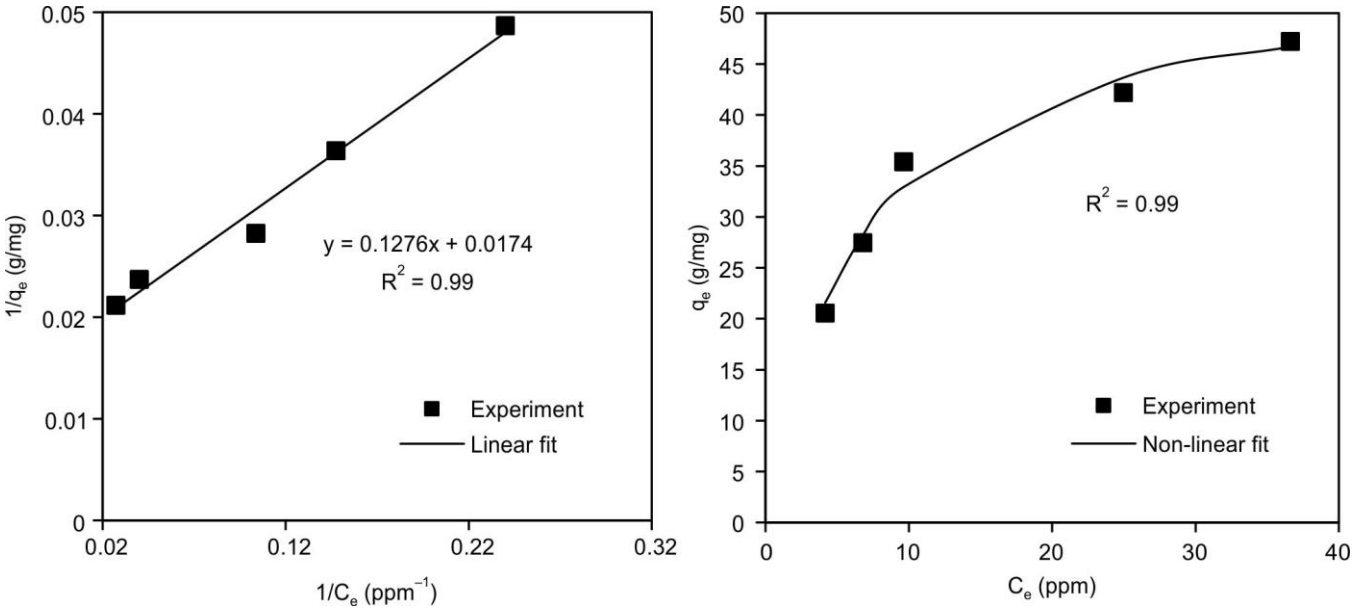

Fig. 9. Linear and non-linear plots for Langmuir isotherm for the adsorption of carmoisine dye by AWAB carbonized at 700 ºC

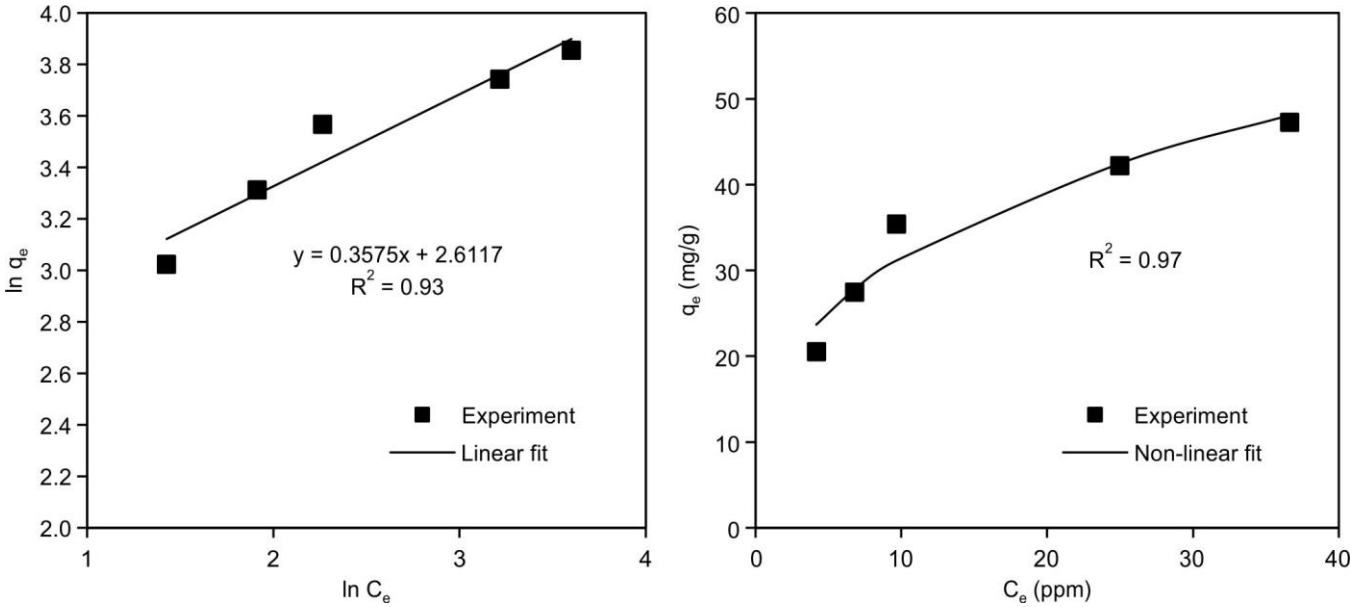

Fig. 10. Linear and non-linear plots for Freundlich isotherm for the adsorption of carmoisine dye by AWAB carbonized at 700 ºC

TABLE-2
PARAMETERS OF LANGMUIR AND FREUNDLICH MODELS FOR THE ADSORPTION OF CARMOISINE DYE ONTO AWAB

Model	Carbonization temperature (°C)	Linear model			Non-linear model		
		K_L (L/mg)	q_m (mg/g)	R^2	K_L (L/mg)	q_m (mg/g)	R^2
Langmuir	500	0.07	58.8	0.96	0.10	49.8	0.97
	600	0.09	61.0	0.94	0.12	56.1	0.96
	700	0.14	57.5	0.99	0.13	63.8	0.99
		K_F (mg/g)	b_F	R^2	K_F (mg/g)	b_F	R^2
Freundlich	500	8.76	0.43	0.87	10.5	0.37	0.94
	600	10.7	0.40	0.85	12.5	0.35	0.93
	700	13.6	0.36	0.93	14.9	0.33	0.97

ated can be used to describe the adsorption process. The Langmuir isotherm assumes that during the adsorption process, each site can accommodate only one molecule of the adsorbate. Furthermore, it is assumed that there is no trans-migration and interaction between adsorbed molecules [15, 21]. The maximum adsorption occurs when the monolayer of adsorbate molecules becomes saturated on the adsorbent surface and has constant energy of adsorption. The maximum

adsorption capacity (q_m) was evaluated to be in the range of 49.8-63.8 mg/g, according to the non-linear model. The reported adsorption capacity is higher than that of Labiod *et al*. [13], who reported a capacity in the range of 7.75-24.2 mg/g when using diatomite as an adsorbent. Saloglu & Sahin [6] reported a q_m of 50 mg/g when using Spirulina algae biomass beads as adsorbent. There is an observed increase in adsorption capacity as the temperature of carbonization is increased. This may be attributed to an increase in the number of active sites. There can be an increase in positive charges on the surface of the adsorbent that enhances the adsorption of dye anions, this observation corroborates with the earlier observation of the decrease of pH_{pzc} of the adsorbent as the temperature of carbonization was increased. The Freundlich isotherm was developed to model the multilayer adsorption on heterogeneous surfaces. It is assumed that there is non-uniform distribution of adsorption heat and affinities over the heterogeneous surface [15,29]. The evaluated values of b_F (0.33-0.37) are less than unity, indicating that the process of adsorption of carmoisine dye onto the prepared adsorbent is favourable. Furthermore, the large K_F values are an indication that there is a strong interaction between the dye and adsorbents. However, the K_F is not a direct measure of the adsorption capacity. There is a decrease in the magnitude of b_F and an increase in the value of K_F as the temperature of carbonization of adsorbents is increased, this implies that the surface heterogeneity of the adsorbent is affected.

Kinetics analysis: Linear and non-linear plots for pseudo-first and second order kinetics analysis for the adsorption process using adsorbent synthesized by carbonizing at 700 ºC are presented in Figs. 11 and 12, respectively. Notably, at low concentrations, the adsorption kinetics fit both pseudo-first and second order kinetics. This implies that at low dye concentrations, the adsorption process is governed by both physical and chemical mechanisms. As the dye concentration increases, the adsorption kinetics are better described by the pseudo-second-order model, as evidenced by the high coefficients of determination presented in Table-3. Furthermore, the parameters obtained from linear and non-linear models for pseudo-second-order kinetics are in good agreement. These results are consistent with the previous works that focused on the use of low-cost adsorbents where pseudo-second-order kinetics with low k_2 values were reported [13,15,30]. The pseudo-second-order kinetics model assumes that the adsorption occurs *via* chemisorption, where the rate of adsorption depends on the surface area of the adsorbents, available adsorption sites and the dye concentration. From Table-3, according to the pseudo-second-order model, in the dye concentration range (75-150 ppm), there is no observed change in the kinetic parameters due to adsorbent carbonization temperature.

Adsorption mechanisms: Kinetics analysis revealed that the adsorption of carmoisine dye onto the adsorbents followed pseudo-first and second order kinetic models at low dye concentrations. However, at higher concentrations, the kinetics were entirely pseudo-second order. This implies that the adsorption process is governed by both physical and chemical mechanisms at low dye concentrations and mainly chemical mechanisms at high dye concentrations. Physical mechanisms involve the creation of forces of attraction between molecules, which can occur through hydrogen bonding, van der Waals forces as well as π^+–π electron donor-acceptor, dipole/induced dipole and quadrupole interactions [14]. The most common chemical mechanism involves electrostatic interactions between the protonated oxygen functional groups of the adsorbents and the –OH and R–SO_3^- groups of the dye. By analyzing the FTIR spectra, it is seen that two new peaks at 1438 cm^{-1} and 1368 cm^{-1} (assigned to the dye's N=N, S=O groups, respectively) appear in the spectrum of the AWAB after the adsorption process, thereby confirming the adsorption of dye onto AWAB. This observation supports the mechanism involving the electrostatic interactions between negatively charged R–SO_3^- ions of the dye and the positively charged adsorbent surface. At low pH values, the protonation of –OH

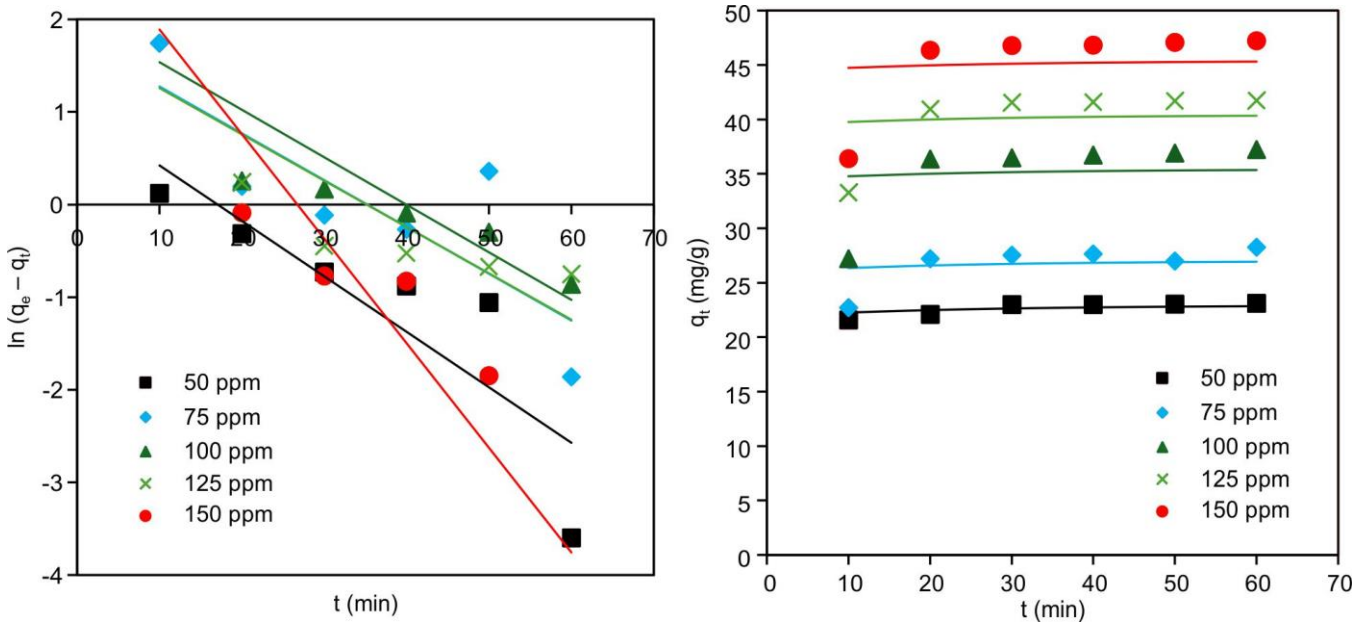

Fig. 11. Linear and non-linear plots for pseudo-first-order kinetics for the adsorption of carmoisine dye onto AWAB carbonized at 700 ºC

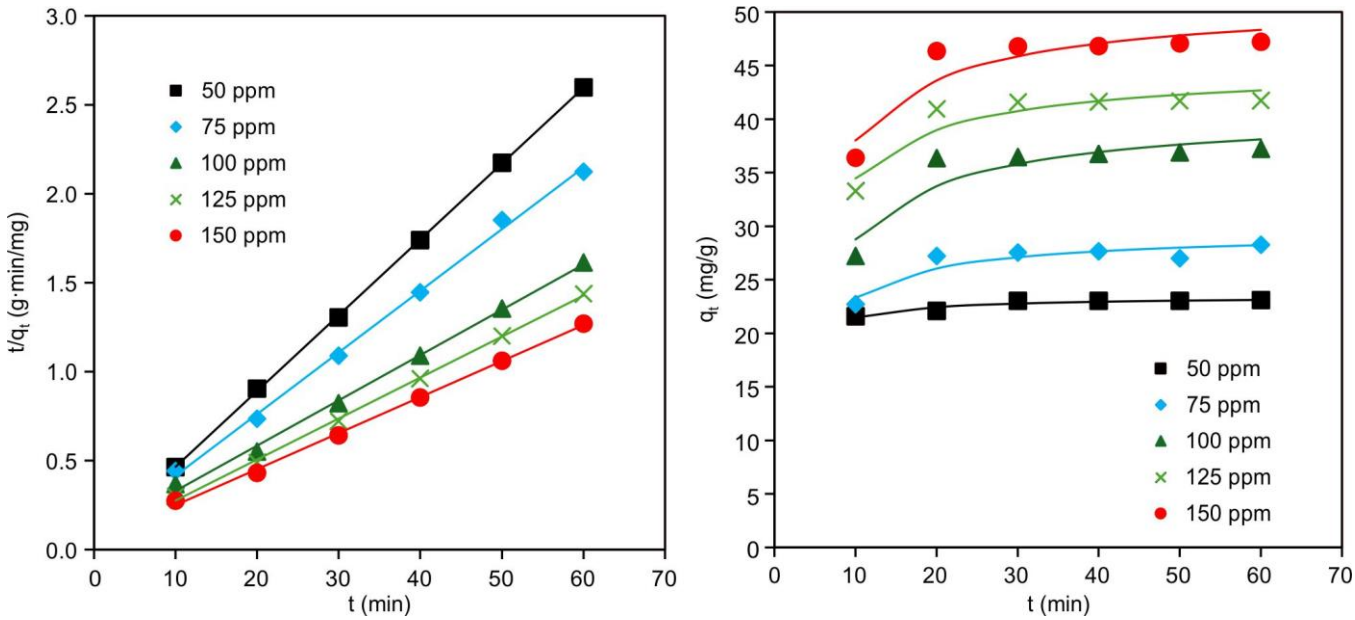

Fig. 12. Linear and non-linear plots for pseudo-second-order kinetics for the adsorption of carmoisine dye onto AWAB carbonized at 700 ºC

TABLE 3
PARAMETERS OF PSEUDO-FIRST AND SECOND ORDER MODELS FOR THE ADSORPTION OF CARMOISINE DYE ONTO AWAB

Model	Carbonization temp. (ºC)	Concentration (ppm)									
		50		75		100		125		150	
		k_1 (min^{-1})	R^2	k_1 (min^{-1})	R^2	k_1 (min^{-1})	R^2	k_1 (min^{-1})	R^2	k_1 (min^{-1})	R^2
Linear model											
Pseudo-1st order	500	0.08	0.96	0.08	0.82	0.09	0.92	0.06	0.78	0.04	0.63
	600	0.05	0.79	0.07	0.86	0.06	0.77	0.05	0.79	0.08	0.80
	700	0.06	0.73	0.05	0.69	0.05	0.76	0.05	0.66	0.11	0.89
Pseudo-2nd order	500	0.06	1.00	0.02	1.00	0.01	1.00	0.01	1.00	0.01	1.00
	600	0.08	1.00	0.02	1.00	0.01	1.00	0.01	1.00	0.01	1.00
	700	0.05	1.00	0.02	1.00	0.01	1.00	0.01	1.00	0.01	1.00
Non-linear model											
Pseudo-1st order	500	0.04	0.98	0.04	0.89	0.04	0.86	0.07	0.91	0.04	0.88
	600	0.03	0.95	0.04	0.89	0.04	0.88	0.04	0.87	0.04	0.85
	700	0.04	0.95	0.04	0.86	0.04	0.86	0.04	0.87	0.04	0.86
Pseudo-2nd order	500	0.07	0.99	0.01	0.95	0.01	0.92	0.01	0.93	0.01	0.94
	600	0.10	0.92	0.01	0.95	0.01	0.94	0.01	0.92	0.01	0.92
	700	0.05	0.95	0.01	0.92	0.01	0.92	0.01	0.93	0.01	0.93

and –COOH groups present in the AWAB surface occurs, resulting in a net positive surface charge. The pH_{pzc} of the adsorbent was found to be in the range of 6.3-6.6, below which the adsorbent surface is positive. There is an observed distinct change in the wavenumber and intensity of the peaks that appear in the range of 2383-2083 cm^{-1}. This indicates that N=C=N and –C=O groups from carbodiimide and lactonic or carboxylic acid, respectively, are involved in the adsorption process. The peak at 1438 cm^{-1}, attributed to the –N=N– group from the dye, occurs at a lower wave number, and this indicate hydrogen bond formation between the O–H groups of AWAB and –N=N– groups of the dye molecules. There is no observed significant change in the original peak at 1552 cm^{-1}, therefore, there is little possibility of π–π electron staking between the C=C double bond in the dye's benzene rings and the delocalized electrons of the adsorbent (Fig. 13).

Based on the FTIR findings, we propose that the interaction between dye molecules and the prepared adsorbents is based on (i) hydrogen bonding involving –OH, –N=C=N–, –C=O and –N=N– groups, as well as (ii) electrostatic interactions between negatively charged $R–SO_3^-$ groups of the dye and the positively charged adsorbent surface that result from the protonation of oxygen atoms on the surface of the adsorbent as shown in Fig. 14.

Conclusion

The present study effectively demonstrated the potential of biochar synthesized from the African wattle tree (*Peltophorum africanum*) bark as an efficient adsorbent for the removal of carmoisine dye from a lab-created mixture that mimics the real wastewater's composition and properties. The findings suggest that the carbonization temperature plays a

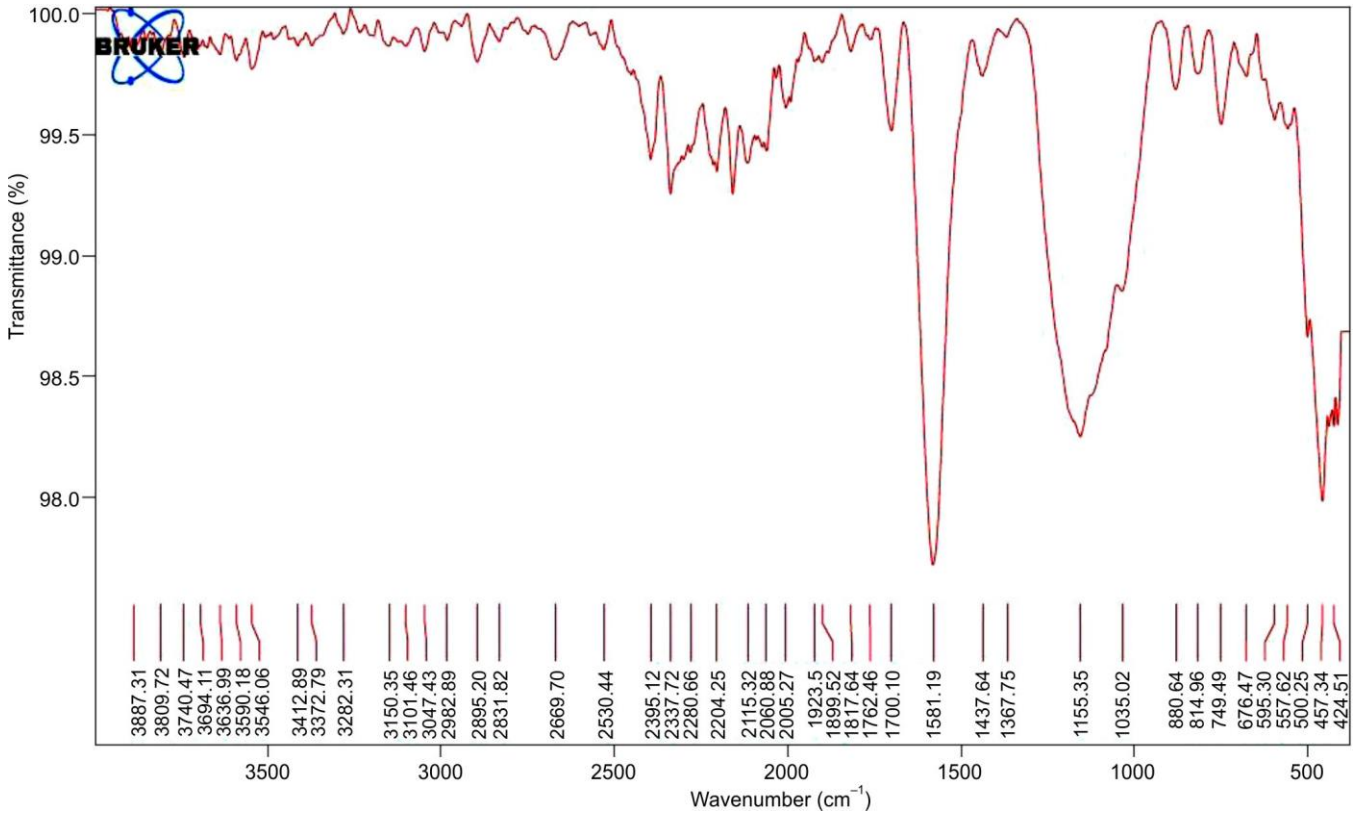

Fig. 13. FTIR spectrum of AWAB after adsorption of carmoisine dye

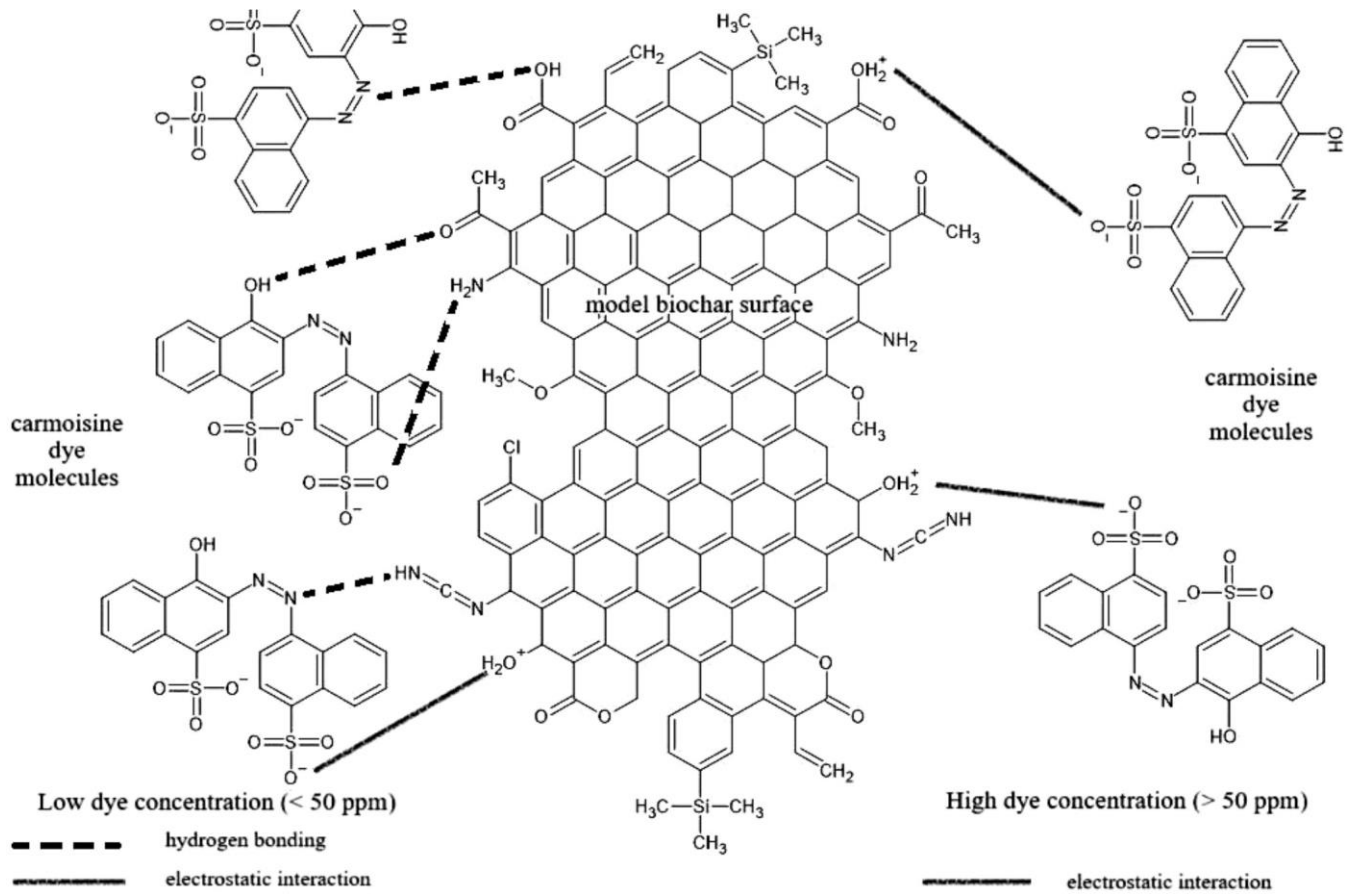

Fig. 14. Possible mechanisms for the adsorption of carmoisine dye onto AWAB

higher temperatures leading to a more positively charged surface. This shift in surface charge altered the adsorption efficiency, as evidenced by the decline in % dye removal with increasing solution pH. Moreover, the adsorption process was found to best fit the Langmuir isotherm model, suggesting monolayer adsorption on the biochar surface, with the highest adsorption capabilities observed for biochar prepared at 700 ºC. Kinetic studies uncovered that the adsorption reaction generally followed pseudo-second-order kinetics, further supporting the involvement of chemisorption. The most likely adsorption mechanisms were recognized as hydrogen bonding and electrostatic interactions, enabled by the presence of carbon-oxygen and carbon-nitrogen functional groups on the surface of biochar. These results suggest that biochar derived from African wattle tree bark is a promising affordable material for the removal of textile dyes from wastewater, with its effectiveness determined by the synthesis conditions and adsorption process parameters. Overall, the study provided valuable insights into the utilization of biochar as an effective adsorbent, contributing to the improvement of sustainable water purification solutions for industrial wastewater.

ACKNOWLEDGEMENTS

The authors are grateful to the facilities provided by the Department of Applied Chemistry of National University of Science and Technology, Bulawayo, Zimbabwe and Department of Chemistry of Nelson Mandela University, Gqeberha (Port Elizabeth), South Africa.

CONFLICT OF INTEREST

The authors declare that there is no conflict of interests regarding the publication of this article.

REFERENCES

1. D.C. Carrascal-Hernández, E.J. Orozco-Beltrán, D. Insuasty, E. Márquez and C.D. Grande-Tovar, *Int. J. Mol. Sci.*, **26**, 7973 (2025); https://doi.org/10.3390/ijms26167973
2. B. Lellis, C.Z. Favaro-Polonio, J.A. Pamphile and J.C. Polonio, *Biotechnol. Res. Innov.*, **3**, 275 (2019); https://doi.org/10.1016/j.biori.2019.09.001
3. H. Kolya and C.H. Kang, *Toxics*, **12**, 111 (2024); https://doi.org/10.3390/toxics12020111
4. A. Das and A. Mukherjee, *Int. J. Hum. Genet.*, **4**, 277 (2004); https://doi.org/10.1080/09723757.2004.11885906
5. P. Mpountoukas, A. Pantazaki, E. Kostareli, P. Christodoulou, D. Kareli, S. Poliliou, C. Mourelatos, V. Lambropoulou and T. Lialiaris, *Food Chem. Toxicol.*, **48**, 2934 (2010); https://doi.org/10.1016/j.fct.2010.07.030
6. D. Saloglu and O.I. Sahin, *Desalination Water Treat.*, **220**, 431 (2021); https://doi.org/10.5004/dwt.2021.27010
7. R. Ganjoo, C. Verma, A. Kumar and M.A. Quraishi, *Adv. Colloid Interface Sci.*, **311**, 102832 (2023); https://doi.org/10.1016/j.cis.2022.102832
8. A. Sadeghi, M.A. Ehrampoush, M.T. Ghaneian, A.A. Najafpoor, H. Fallahzadeh and Z. Bonyadi, *Desalination Water Treat.*, **137**, 273 (2019); https://doi.org/10.5004/dwt.2019.23189
9. M.M. Biswas, K.E. Taylor, J.K. Bewtra and N. Biswas, *Water Environ. Res.*, **79**, 351 (2007); https://doi.org/10.2175/106143006X111727
10. Y. Fu and T. Viraraghavan, *Bioresour. Technol.*, **79**, 251 (2001); https://doi.org/10.1016/S0960-8524(01)00028-1
11. S. Moyo, B.P. Makhanya and P.E. Zwane, *Heliyon*, **8**, e09632 (2022); https://doi.org/10.1016/j.heliyon.2022.e09632
12. A. Mathur, C. Ghosh, P. Roy, R. Prasad and R.P. Singh, *Adv. Microbiol.*, **14**, 137 (2024); https://doi.org/10.4236/aim.2024.142011
13. K. Labiod, S. Hazourli, M. Bendaia, M. Tlili, A. Aitbara, R. Graine and H. Meradi, *Adsorpt. Sci. Technol.*, **2022**, 9517605 (2022); https://doi.org/10.1155/2022/9517605
14. M. Vithanage, S.S. Mayakaduwa, I. Herath, Y.S. Ok and D. Mohan, *Chemosphere*, **150**, 781 (2016); https://doi.org/10.1016/j.chemosphere.2015.11.002
15. G. Mapombere, B. Nyoni, L.L. Sibali, H. Chiririwa and T. Sedibeng, *Iran. J. Chem. Chem. Eng.*, **40**, 143 (2022); https://doi.org/10.30492/ijcce.2020.125700.4109
16. M. Leulescu, A. Rotaru, A. Moanţă, G. Iacobescu, I. Pălărie, N. Cioateră, M. Popescu, M.C. Criveanu, E. Morîntale, M. Bojan and P. Rotaru, *J. Therm. Anal. Calorim.*, **143**, 3945 (2021); https://doi.org/10.1007/s10973-021-10618-4
17. K. Mensah, H. Mahmoud, M. Fujii, M. Samy and H. Shokry, *Biomass Convers. Biorefin.*, **14**, 12945 (2024); https://doi.org/10.1007/s13399-022-03304-4
18. H.L. Nicholas, I. Mabbett, H. Apsey and I. Robertson, *Gates Open Res.*, **6**, 96 (2022); https://doi.org/10.12688/gatesopenres.13727.2
19. O.A. Hussain, A.S. Hathout, Y.E. Abdel-Mobdy, M.M. Rashed, E.A. Abdel Rahim and A.S.M. Fouzy, *Toxicol. Rep.*, **10**, 146 (2023); https://doi.org/10.1016/j.toxrep.2023.01.011
20. P.R. Rout, P. Bhunia and R.R. Dash, *Desalination Water Treat.*, **2014**, 1 (2014); https://doi.org/10.1080/19443994.2014.881752
21. L.L. Borba, R.M.F. Cuba, F.J.C. Teran, M.N. Castro and T.A. Mendes, *Braz. Arch. Biol. Technol.*, **62**, e19180450 (2019); https://doi.org/10.1590/1678-4324-2019180450
22. S. Deshmukh, N.S. Topare, S. Raut-Jadhav, P.V. Thorat, S.A. Bokil and A. Khan, *AQUA Water Infrastruct. Ecosyst. Soc.*, **71**, 1351 (2022); https://doi.org/10.2166/aqua.2022.119
23. A.S. Materiienko, V.A. Grudko, V.A. Khanin and V.A. Georgyiants, *Pharma Chem.*, **7**, 237 (2015).
24. S.N. Guilhen, T. Watanabe, T.T. Silva, S. Rovani, J.T. Marumo, J.A.S. Tenório, O. Mašek and L.G. Araujo, *Recent Prog. Mater.*, **4**, 1 (2022); https://doi.org/10.21926/rpm.2202010
25. N. Saha, A. Saba and M.T. Reza, *J. Anal. Appl. Pyrolysis*, **137**, 138 (2019); https://doi.org/10.1016/j.jaap.2018.11.018
26. S. Liu, Y. Ding, P. Li, K. Diao, X. Tan, F. Lei, Y. Zhan, Q. Li, B. Huang and Z. Huang, *Chem. Eng. J.*, **248**, 135 (2014); https://doi.org/10.1016/j.cej.2014.03.026
27. R. Lafi, I. Montasser and A. Hafiane, *Adsorpt. Sci. Technol.*, **37**, 160 (2019); https://doi.org/10.1177/0263617418819227
28. M.A. Hossain, H.H. Ngo and W. Guo, *J. Water Sustain.*, **3**, 223 (2013).
29. H. Chiririwa, T. Matthews, B. Nyoni, S. Majoni and B. Naidoo, *Asian J. Chem.*, **29**, 2761 (2017); https://doi.org/10.14233/ajchem.2017.20877
30. M. Zabihi, A. Haghighi Asl and A. Ahmadpour, *J. Hazard. Mater.*, **174**, 251 (2010); https://doi.org/10.1016/j.jhazmat.2009.09.044